Importance of Madden–Julian Oscillation phase to the interannual variability of East African rainfall

Received: 22 July 2022 | Revised: 14 November 2022 | Accepted: 24 November 2022

DOI: 10.1002/asl.1148

RESEARCH ARTICLE

Atmospheric Science Letters RMetS

Importance of Madden–Julian oscillation phase to the interannual variability of East African rainfall

Ben Maybee[1] | **Neil Ward**[1] | **Linda C. Hirons**[2] | **John H. Marsham**[1]

[1]School of Earth and Environment, University of Leeds, Leeds, UK

[2]National Centre of Atmospheric Science (NCAS), University of Reading, Reading, UK

Correspondence
Ben Maybee, School of Earth and Environment, University of Leeds, Leeds, UK.
Email: b.w.maybee@leeds.ac.uk

Funding information
Global Challenges Research Fund, Grant/Award Number: NE/P021077/1 (GCRF African SWIFT); Natural Environment Research Council, Grant/Award Number: NE/M02038X/1 (FCNO/NERC HyCristal)

Abstract

Precipitation across East Africa shows marked interannual variability. Seasonal forecast skill for the OND short rains is significantly higher than for the MAM long rains, which also exhibit poorly understood decadal variability. On sub-seasonal time-scales rainfall is influenced strongly by the phase of the Madden–Julian Oscillation (MJO); here we investigate whether this influence extends to interannual and decadal scales. We show that the number of days that the MJO is active and in phases 1–3 has a greater influence than the mean amplitude of the MJO on interannual long rains variability ($\rho = 0.59$ for the count of phases 1–3, compared to $\rho = 0.40$ for amplitude). The frequency of these days is linked to a newly identified gradient in Pacific sea-surface temperatures (SSTs), whose influence on long rains variability we show is itself mediated by the MJO. We develop a statistical model estimating East African rainfall from MJO state, and show that the influence of the MJO on seasonal rainfall extends to the short rains, and to a lesser extent also into January and February. Our results show the importance of capturing the SST-MJO phase relationship in models used for predictions of East African rainfall across time-scales, and motivate investigating this further.

KEYWORDS

East African rainfall, interannual variability, MJO

1 | INTRODUCTION

East Africa (EA) has an extensive equatorial region broadly exhibiting two main rainy seasons per year, the March–May (MAM) long rains (LR) and October–December (OND) short rains (SR) (Dunning et al., 2016; Nicholson, 2017; Yang et al., 2015). All seasons have significant interannual variability of rainfall, with considerable socio-economic impacts on populations (FEWS NET Alert, 2021; Funk, 2020; Funk et al., 2018; Lyon, 2014; Wainwright et al., 2021). Longer term decadal variability is also notable, with an apparent decline in LR precipitation over much of the Horn of Africa during the early 2000s—in apparent contrast to climate model projections—labelled the East African rainfall paradox (Lyon & DeWitt, 2012; Rowell et al., 2015). The observed drying can be explained by a strengthened zonal gradient in western Pacific sea-surface temperatures (SSTs) (Hoell & Funk, 2014; Liebmann et al., 2014), attributed to both natural Pacific decadal variability and anthropogenic forcings (Bahaga et al., 2019; Funk et al., 2018; Hoell & Funk, 2014; Liebmann et al., 2017; Lyon, 2014; Rowell et al., 2015; Williams & Funk, 2011; Yang

et al., 2014). In recent years rainfall appears to have somewhat recovered, but with high interannual variability (Kilavi et al., 2018; Wainwright et al., 2019; Wainwright et al., 2021; Walker et al., 2020).

Predictions of EA seasonal rainfall have enabled early action, saving lives (Funk et al., 2018; Hillbruner & Moloney, 2012; Sheffield et al., 2014). Seasonal predictions, either from dynamical or statistical models, are more skilled for SR than LR rainfall; for example, Walker et al. (2019) reported a correlation of 0.69 for Met Office GloSea5 short rains predictions, but a LR value of 0.07. This discrepancy is largely because of control by the Indian Ocean Dipole (IOD) during the short rains (Black et al., 2003; Hirons & Turner, 2018; MacLeod, Graham, et al., 2021; Walker et al., 2019). Some dynamical models do have skill for the LR (MacLeod, 2019), while moderately skillful statistical models for the LR have been constructed (Nicholson, 2014), with predictions based on Indo-Pacific SSTs enabling early warnings of EA drought events in all seasons (Funk et al., 2014, 2018).

Global models' sub-seasonal skill has recently improved, enabling accurate predictions of EA rainfall on the time-scale of weeks; this is in part due to improved model representation of the Madden–Julian Oscillation (MJO), and also to improved understanding of the impacts of the MJO on local East African weather (Zaitchik, 2017; de Andrade et al., 2021; MacLeod, Dankers, et al., 2021;Vashisht & Zaitchik, 2022). The MJO (Madden & Julian, 1971, 1972) plays a well-established role in the intraseasonal variability of rainfall across EA, with phases 1–4 (5–8) generally associated with wet (dry) anomalies through both rainy seasons (Berhane & Zaitchik, 2014; Hogan et al., 2015; Omeny et al., 2008; Pohl & Camberlin, 2006a). These relationships are typically well captured by models, excepting some heterogeneity across the region (Hogan et al., 2015; MacLeod, Dankers, et al., 2021). There is an inherent asymmetry between the rainy season wet and dry phases, with the MJO driving larger wet anomalies than dry (Pohl & Camberlin, 2006a; Vellinga & Milton, 2018), and notable examples exist of large amplitude MJO events contributing to the onset of extreme wet periods over EA (Kilavi et al., 2018; MacLeod, Dankers, et al., 2021; Wainwright et al., 2021).

Intriguingly, it has been found that the amplitude of the MJO plays an important role in LR interannual variability (Pohl & Camberlin, 2006b; Vellinga & Milton, 2018), with $\rho = 0.51$ during March–April when regressing mean MJO amplitude against the leading principal component of EA rainfall (Vellinga & Milton, 2018). EA rainfall has been linked to anomalous westerlies bringing moist air from the Congo basin (Finney et al., 2020), which are themselves linked to the MJO (Berhane & Zaitchik, 2014). Recently, Walker et al. (2020) showed that variations in the westerly winds have influenced LR variability on both decadal and interannual time-scales, and that a similar, albeit reduced, influence existed for the mean MJO amplitude.

The role of the MJO in notably wet years (Kilavi et al., 2018; Vellinga & Milton, 2018; Wainwright et al., 2021), and the recently identified role of MJO variability in some tropical rainfall trends (Roxy et al., 2019), raises the question to what extent EA interannual, and decadal, rainfall variability can be explained by its state. The MJO is known to be influenced by Indo-Pacific SSTs (Liu et al., 2016; Pang et al., 2016; Pohl & Matthews, 2007; Slingo et al., 1999; Suematsu & Miura, 2018), with substantial control of the MJO life-cycle (Dasgupta et al., 2021; Roxy et al., 2019). Understanding SST controls of the MJO during the long rains, and to what extent SST influences on EA are expressed through the MJO, should provide insight into factors which must be represented to accurately model and predict EA rainfall. This paper therefore, after defining our methods and study region (Section 2), first considers the role of the MJO (especially life-cycle phases) in the LR (Section 3.1), further examining relationships with Pacific SSTs. We then consider the MJO's role across all seasons (Section 3.2), before presenting our conclusions (Section 4).

2 | DATA AND METHODS

We use daily Climate Hazards Center InfraRed Precipitation with Station data (CHIRPS) rainfall data at 0.05° grid resolution, spanning 1981–2019. CHIRPS combines infrared satellite estimates of tropical precipitation with a global network of tropical ground-based gauges (Funk et al., 2015). We have repeated appropriate analyses using daily rainfall from the Integrated Multi-satellitE Retrievals for GPM (IMERG) algorithm, for which data are only available from 2000.

Results shown for Pacific SSTs use the Met Office HadSST dataset (Rayner et al., 2003) of monthly global SSTs at 1° grid resolution; we have repeated our analyses using the National Oceanic and Atmospheric Administration (NOAA) Extended Reconstruction SST and Optimum Interpolation datasets, finding similar conclusions. The latter dataset underpins the monthly NOAA SSTOI anomaly indices computed for all Niño regions, which we use to determine relationships with ENSO. To study the state of the MJO we use the Wheeler–Hendon (WH) indices generated daily by the Bureau of Meteorology. The WH indices RMM1 and RMM2 (Wheeler & Hendon, 2004) are computed as the leading empirical orthogonal functions of combined near-equatorially

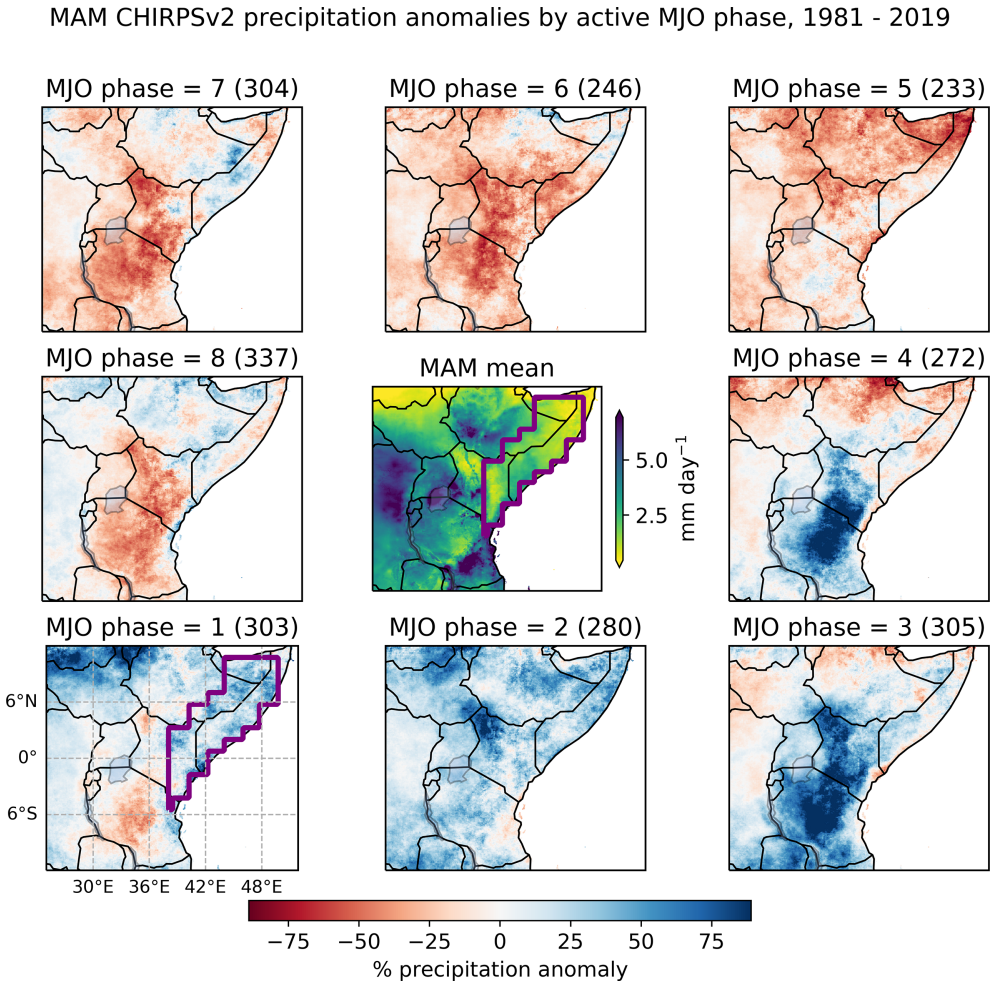

FIGURE 1 Effect of MJO phase on intraseasonal variability of east African rainfall. Boundary plots show mean MAM percentage precipitation anomalies over EA grouped by active MJO phase, with number of days occurring from 1981 to 2019 given in parentheses. Central plot displays mean MAM precipitation over all days. Thick solid purple lines in plots show primary EA study region

averaged zonal winds and NOAA satellite observations of outgoing longwave radiation (Liebmann & Smith, 1996).

MJO amplitude and phase are computed as the norm and arctangent of the RMM indices, respectively. An amplitude greater than 1 indicates an active MJO, while the eight phases capture the MJO's life-cycle (Wheeler & Hendon, 2004). Figure 1 shows how MAM precipitation anomalies across EA depend on this cycle, with wet anomalies typically appearing in phases 1–3, when the MJO convective core is located over the Indian Ocean. We measure the frequency of such events in a given period by counting the number of days in which the MJO is both active and in phases 1–3; we label this measure MJO123, and refer to such days as EA wet-phase days.

To capture the effects of the full range of MJO amplitudes and phases on EA rainfall, we generate a model rainfall index dependent solely on MJO state. Our method uses the WH dataset to allocate daily mean percentage rainfall anomalies to phase and amplitude bins. We then compute the mean anomaly for each bin, group bins by phase, and apply weighted linear regression, yielding a fit function $\hat{r}(\theta, |\mathrm{RMM}|^2)$ comprising eight monotonic series of percentage rainfall anomalies. The rainfall estimate $r_{\mathrm{est}}(t)$ is computed by applying such a fit-function to the mean daily climatological rainfall $\overline{r}_d$,

$$r_{\mathrm{est}} = \overline{r}_d + \hat{r}(\theta, |\mathrm{RMM}|^2) \cdot \overline{r}_d. \quad (1)$$

The index r_{est} forms a daily time-series, since it depends ultimately on the WH indices RMM1 and RMM2. We refer to r_{est} as an RMM estimate (of precipitation). In generating the fit function one may calculate independent fits over intervals of the year; we use seasonal fits, so $\hat{r}$ comprises 32 independent linear fits (one for each MJO phase in each season). We also use $\pi/4$ phase bins with an amplitude width of 0.5, and require bins to contain at least three data points for inclusion in the regression, which is weighted to the standard error of the bin means.

Our main study region is the bold outlined area in Figure 1, since this region (which we henceforth label East Africa) is associated with distinct bimodal annual rainfall and recent decadal LR drying trends (Liebmann et al., 2017). Unless stated otherwise, the study period for all results is 1981–2019. In keeping with previous

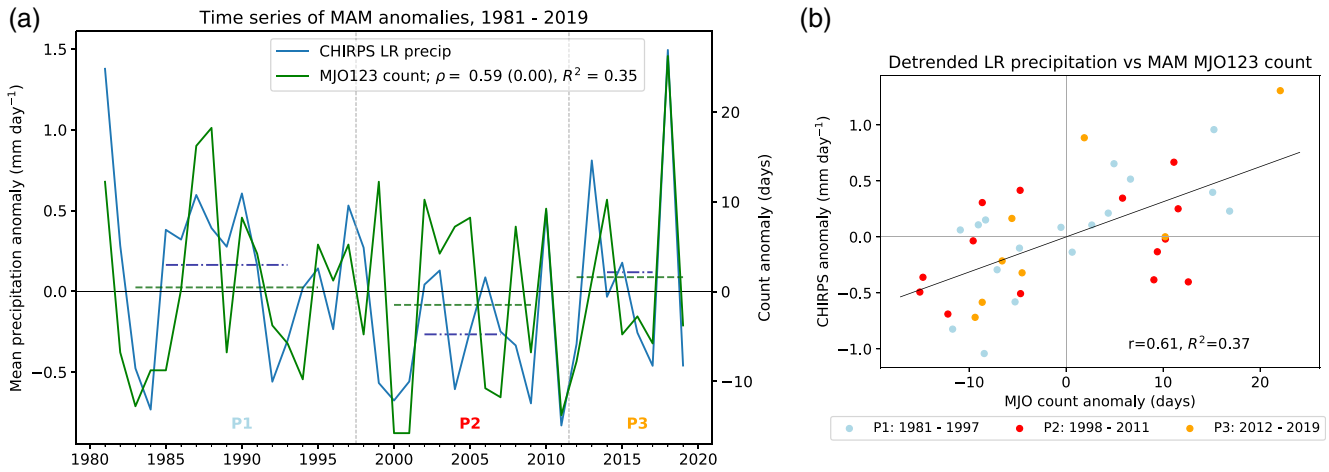

FIGURE 2 Variation of LR precipitation and EA MJO wet-phase frequency. (a) Time series of anomalies of CHIRPS LR precipitation (MAM rainfall over EA; blue) and counts of active MJO phase 1–3 days (MJO123 count, green); anomalies are calculated about full study-period mean (1981–2019). Correlation between variables is $\rho = 0.59$ ($p = 0.00$), with $R^2 = 0.35$. Green dashed (blue dot-dashed) horizontal lines show MJO123 count (EA precipitation) decadal means for sub-periods P1, P2 and P3 (labelled). (b) Scatter plot of the same variables with cubic polynomial trends removed (i.e., detrended), with data-points grouped by decadal sub-periods. Black line is linear regression line fitted to points. Correlation values after detrending are $\rho_{dt} = 0.61$ (0.00), $R^2 = 0.37$

analyses of the LR drying trend (Wainwright et al., 2019; Walker et al., 2020), we define wet, dry, and recovery sub-periods; these are 1981–1997 (P1), 1998–2011 (P2) and 2012–2019 (P3), respectively (Figure 2).

To separate interannual and decadal variability, we follow Walker et al. (2020) and apply linear regression to datasets from which long-term trends are removed by fitting, and removing, a cubic polynomial. Hereafter, such filtered series are referred to as detrended. The expected change in mean rainfall between P1 and P2 due to the observed change in the state of an external variable is calculated as the product of the gradient of the regression line and the observed change in variable mean from P1 to P2 (equation 1 of Walker et al., 2020). If the expected change in mean rainfall between P1 and P2 is approximately equal to the observed decadal change, then this supplies evidence that the mechanism linking rainfall and external variables on interannual time-scales also holds on decadal time-scales.

We calculate the Pearson correlation coefficient (ρ) for key indices, with p-values for significance estimated using a two-sided t-test. Full degrees of freedom are assumed, since key indices do not contain significant serial correlation. Correlations taken after first applying the cubic polynomial filter to indices are referred to as detrended correlations (ρ_{dt}). To test for mediation in the relationships of causal variables we use the regression framework outlined in Kolstad and MacLeod (2022). The statistical significance of composite mean differences is estimated using a Welch t-test without assumption of equal sample variance.

3 | RESULTS

3.1 | Interannual variability of the EA long rains

The time-series values of LR precipitation and MAM MJO123 (Figure 2a) are strongly correlated ($\rho = 0.59$, $p < 0.01$), and this is maintained after detrending (Figure 2b, $\rho_{dt} = 0.61$). The MAM counts for each phase alone (1, 2, 3) are also significantly correlated with LR precipitation, but MJO123 gives the strongest result. In contrast, the MAM count for phases 5–7 has no association with LR precipitation ($\rho = 0.03$, $\rho_{dt} = 0.12$). The MAM count of all active days is significantly correlated with LR precipitation ($\rho = 0.42$, $\rho_{dt} = 0.47$, both $p < 0.01$) but substantially reduced compared to the correlation with MJO123 count. Likewise, for the mean MAM MJO amplitude (all days) $\rho = 0.40$ ($\rho_{dt} = 0.44$), while restricting to phases 1–3, $\rho = \rho_{dt} = 0.37$.

The drying trend in LR precipitation between P1 and P2 is clear (Figure 2a), whereas the decline in MJO123 count is far less striking. Applying a t-test to the mean values in P1 and P2 (indicated with horizontal lines in Figure 2a), precipitation change is highly significant, whereas MJO123 is far from significant.

To provide a quantification of the contribution of the MJO123 count to decadal LR variability, the approach of Walker et al. (2020) is applied. First, the detrended values of MAM MJO123 (m) are regressed onto LR precipitation (r). The regression line (Figure 2b) is $r = 0.03\ m + 0.00$, where the standard slope error $\sigma_{slope} = 0.01$ mm day^{-1}.

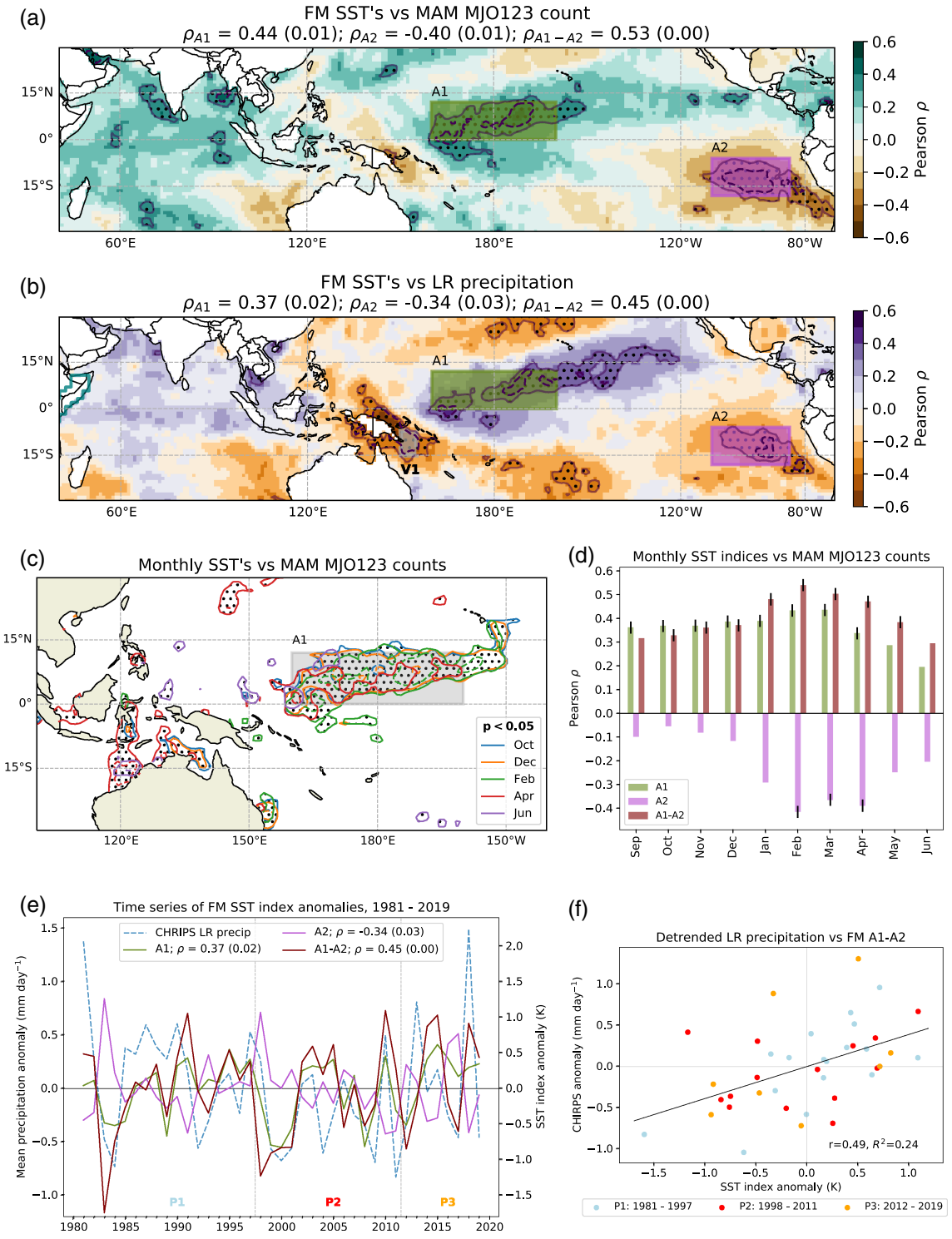

FIGURE 3 Relationships between indo-Pacific SSTs, MAM MJO123 count and LR precipitation (a) correlations for FM mean SSTs vs MAM MJO123 counts; significant values ($p < 0.05$) are denoted by stippling, with further interior dashed contours where $p < 0.01$. Rectangles A1 and A2 indicate regions used to calculate SST indices. Correlations (and p-value significance) between the MAM MJO123 counts and SST indices reported in legend. (b) Repeated vs mean LR precipitation. Rectangle V1 (east of New Guinea) is also used to calculate a western Pacific SST index. Turquoise solid line over Africa indicates EA study region. (c) Central and western Pacific contours of significant monthly SST correlations against MAM MJO123, with stippling and solid (interior dashed) contours for 95% (99%) significance; for boreal winter months, values are taken against month preceding MAM. (d) Monthly correlation values for SST indices against MAM EA wet-phase days. A1 (A2) values shown in green (pink), A1 − A2 in red. Markers on bars indicate significant values; boreal winter months again precede MAM. (e) Time series of FM SST index anomalies (same colours as in (d)) and LR precipitation (blue); correlations with LR precipitation reported in legend. (f) Regression of detrended FM index A1 − A2 onto detrended LR precipitation anomalies. Regression line shown; $\rho_{dt} = 0.49$ (0.00), with $R^2 = 0.24$

The observed decline in mean rainfall from P1 to P2 is $\Delta r_{obs} = -0.43 \pm 0.10$ mm day^{-1}, while the change in the mean MJO123 count is -1.95 ± 3.96 days. From the regression equation, this amounts to an expected change in rainfall of $\Delta r_{exp} = -0.06 \pm 0.12$ mm day^{-1}; only ~14% of the observed decline in rainfall can thus be attributed to the decadal change in MJO123 count. Repeating for mean MAM MJO amplitude yields a very similar level of variance.

What drives the interannual variability in the MJO123 count? Indo-Pacific warmpool SSTs are known to influence the MJO life-cycle (Dasgupta et al., 2021; Roxy et al., 2019): given the relationship in Figure 2, it is pertinent to understand if any similar mechanism may influence LR variability through the MJO. Figure 3a displays the distribution of correlations between MAM MJO123 counts and mean February–March (FM) SSTs, when the observed correlations are strongest (variations by month discussed later). As is typical for such significance testing, some false rejections of the null hypothesis will occur by chance, hence significance thresholds should be stricter for spatial data (Katz & Brown, 1991; Wilks, 2016)—standard local levels quoted here are for guidance only, while we have also shown contours where $p < 0.01$. The correlations are positive across the bulk of the Indian Ocean, but rarely significant. Instead, the largest area of significant positive correlation lies in the central Pacific, while the only area of significant negative correlation lies in the southeastern Pacific. To quantify this dipole structure we identify two representative regions in Figure 3a, A1 (160°E to 160°W, 0°N to 12°N) and A2 (110°W to 85°W, 18°S to 6°S). We then define three SST indices: A1, A2, and the gradient A1 − A2. Regressing each index calculated over FM against MAM MJO123 count, for A1 (A2) $\rho = 0.42$ (-0.40), $p < 0.05$, while for A1 − A2, $\rho = 0.53$, $p < 0.01$ (all ρ_{dt} values similar).

The corresponding values taken against LR precipitation are $\rho = 0.37$ ($\rho_{dt} = 0.41$) for A1; $\rho = -0.34$ ($\rho_{dt} = -0.38$) for A2; and $\rho = 0.45$ ($\rho_{dt} = 0.49$) for A1 − A2. Again $p < 0.05$ for the indices individually, and $p < 0.01$ for the gradient. Note all values are lower for rainfall than MJO123 count. The corresponding spatial distribution of SST correlations with LR precipitation is plotted in Figure 3b, and again shows a gradient between significant positive (negative) correlation in the central (southeastern) Pacific. The primary difference from Figure 3a is the V-shaped pattern of negative (often significant) correlation in the western Pacific, especially at the apex of the V. A similar pattern has been found in previous studies examining the role of western Pacific SSTs in the LR drying trend (Funk et al., 2018, 2019; Funk & Hoell, 2015; Lyon & DeWitt, 2012). Comparing the distributions suggests that the relationship of western Pacific SSTs with EA rainfall totals is more independent of the MJO. Indeed, taking the FM means for region V1 shown in Figure 3b (150°E to 155°E, 15°S to 7°S), the correlation against LR rainfall is significant ($\rho = -0.47$, $\rho_{dt} = -0.38$), but this is not the case for MJO123, where $\rho = -0.26$ ($\rho_{dt} = -0.28$).

The differing relationships of the SST indices A1 − A2 and V1 to the MJO (and LR precipitation) can be further demonstrated by testing for mediation. First, consider the regression

$$\mathrm{LR} = a_0 + a_1(\mathrm{A1} - \mathrm{A2}) + a_2(\mathrm{MJO123}). \quad (2)$$

The results for this regression (FM A1 − A2, MAM MJO123 count) are reported in Table S1, showing that a_1 is not statistically significant (even though the direct correlation between LR and A1 − A2 is highly significant). Following Kolstad and MacLeod (2022), this result implies that the link between LR and A1 − A2 is mediated through MJO123. In other words, LR precipitation is conditionally independent of A1 − A2, when accounting for the relationship to MJO123. When the analysis is repeated using FM V1 in place of A1 − A2, the coefficient a_1 this time remains significant (Table S2), indicating that the impact of V1 on EA is not mediated through MJO123. Moreover, when regressing the two SST indices against LR (without MJO123; Table S3a), the coefficients for A1 − A2 and V1 are both significant; however as soon as MJO123 is added (Table S3b), the A1 − A2 coefficient is no longer significant. We therefore conclude that both SST indices account for significant independent variability in LR precipitation, but that the MAM MJO123 count contains all (or at least almost all) of the explanatory power of FM A1 − A2.

Considering monthly variations in A1 correlation with MAM MJO123, Figure 3c shows significant correlations starting from the preceding October, beginning to wane in April, and disappearing entirely in June. Similar regions surrounding the Maritime Continent are far less stable. For A2 (not shown) the persistent period is shorter, spanning January to April. Figure 3d quantifies these trends by plotting monthly correlations for the relevant SST indices, showing that correlations peak during FM. The period with strongest correlations is January–April, suggesting seasonal control of the MAM MJO. Similar results hold for correlations against LR precipitation, but with the strongest relationship in April (not shown).

The time-series of the FM SST indices are compared against that for LR precipitation anomalies in Figure 3e. For the SST indices interannual variability is clearly present, but decadal variability less-so. The regression of detrended FM A1 − A2 values against LR rainfall

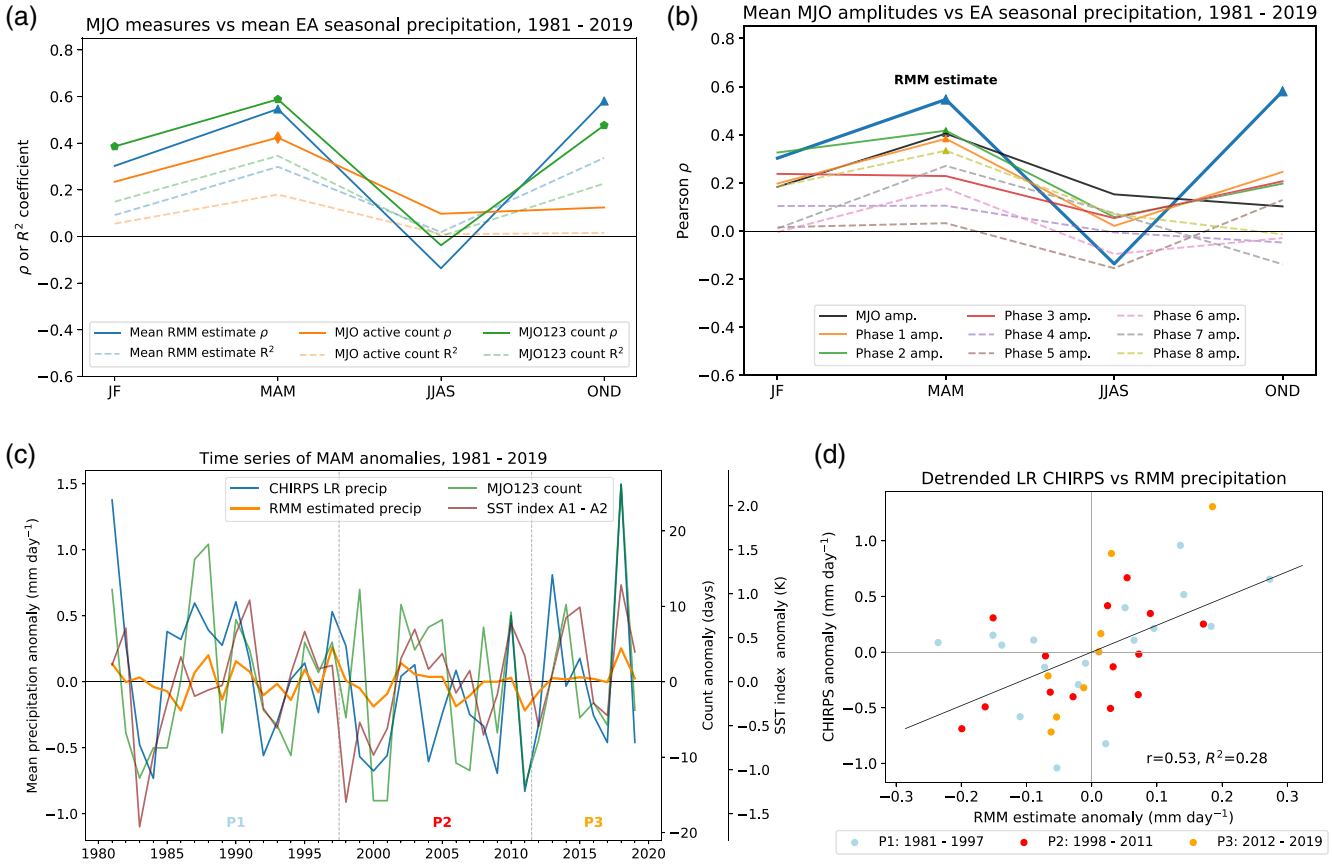

FIGURE 4 Role of MJO phase in all seasons. (a) Pearson ρ and R^2 coefficients for three mean seasonal MJO measures vs EA precipitation (CHIRPS). Measures are the RMM precipitation index (RMM estimate, blue); count of all active MJO days (MJO active count, orange), and MJO123 count (green). Significant correlations are indicated by polygons. (b) Repeated (correlations only) for mean seasonal MJO amplitude across all days (MJO amp., black) and by MJO phase (phases 1–3 solid lines, 4–8 dashed). RMM estimate correlations replotted (blue). (c) Time-series of CHIRPS observed (blue) and RMM estimated (orange) LR precipitation anomalies. Correlation between values is $\rho = 0.58$ (0.00), $R^2 = 0.34$. Also plotted are MAM anomalies of MJO123 counts (green) and SST index A1 − A2 (red). (d) Regression of detrended anomalies for LR precipitation variables, with regression line shown (black). Correlation $\rho_{dt} = 0.53$ (0.00), with $R^2 = 0.28$

(MAM) is shown in Figure 3f; the regression equation is $r = 0.39\,s + 0.00$, $\sigma_{slope} = 0.11$ mm K^{-1}. The change in the decadal mean index from P1 to P2 is $\Delta s = -0.16 \pm 0.19$ K; regressing, the SST index explains only ~15% of the observed decline in LR precipitation. This differs from the decadal influence on LR rainfall exhibited by western Pacific SSTs; for example, applying the same methodology to region V1, around 80% of the LR drying trend is explained.

Regions A1 and A2 lie close to the ENSO regions, with A1 in particular resembling ENSO4 (5°S to 5°N, 160°E to 150°W). There therefore exist significant correlations between the FM ENSO indices and the indices defined here. However, there is no significant correlation between any mean FM ENSO index and either the MAM MJO123 count or LR precipitation; the strongest such relationship is with ENSO4, where $\rho = 0.23$, $p = 0.16$ against both variables.[1] These results agree with previous assessments of the impact of ENSO on LR precipitation (de Andrade et al., 2021), and suggest that the mechanism through which Pacific SSTs influence the MAM MJO and LR precipitation is separate to ENSO.

3.2 | Interannual variability of seasonal EA rainfall

The MJO plays an important role in interannual variability of the EA long rains; does this extend to other seasons? Figure 4a plots the correlation and R^2 coefficients between mean EA seasonal rainfall and three measures of the MJO: mean RMM estimate precipitation index for EA, described in Section 2; mean MJO123 count; and mean count of all active days. The first two measures have similar strength relationships in both MAM and OND, suggesting the MJO explains ~30% of interannual variability of both rainy seasons; lower correlations in January–February (JF) and, especially, June–September

(JJAS), suggest different mechanisms operate in the drier climatology seasons. Monthly statistics give similar results (not shown). The negligible difference between the RMM estimate, fitted to all MJO phases and amplitudes, and simple MJO123 count emphasises the key role played by the frequency of EA wet-phase days in interannual rainfall variability.

The same correlations are plotted for mean seasonal MJO amplitude in Figure 4b. Comparing against the RMM estimate, it is apparent that MJO amplitude has a weaker relationship with EA seasonal rainfall than measures of phase frequency, especially during the short rains. As noted by Kimani et al. (2020), phase 2 magnitude has the strongest relationship, but this is only significant in MAM. We find similar results for monthly means (not shown).

The correlation between the RMM estimated and CHIRPS observed time-series for mean LR precipitation (shown in Figure 4c) is $\rho = 0.58$ ($\rho_{dt} = 0.53$); for both results $p < 0.01$. The decline in correlation after detrending suggests the RMM estimate may have stronger decadal variability than previously considered MJO measures. Figure 4d shows the regression of detrended RMM and CHIRPS LR precipitation anomalies. The regression equation is $r = 2.41 r_{est} + 0.00$, $\sigma_{slope} = 0.63$, and the change in the RMM estimate from P1 to P2 is $\Delta r_{est} = -0.05 \pm 0.05$ mm day^{-1}. Applying the regression equation yields an expected change in rainfall $\Delta r_{exp} = -0.12 \pm 0.13$ mm day^{-1}, or ~28% of the observed change. This is higher than equivalent results for MJO123 or mean amplitude, but still relatively small compared to the standard error.

4 | CONCLUSIONS

We have investigated the role of the phase of the MJO in modulating interannual and decadal variability of the East African long rains. We have shown that the MAM count of days in which the MJO is active and in phases 1–3 (MJO123) has a significant correlation ($\rho = 0.59$) with LR precipitation, and that this relationship is stronger than the relationship with alternative counts of MJO days, or with measures of mean MJO amplitude. After detrending to isolate interannual from decadal variability, the correlation increases to $\rho_{dt} = 0.61$.

The influence of MJO phase on LR variability is not substantial for decadal time-scales. We found that there is a decline in the frequency of MAM MJO123 days from 1981–1997 (P1) to 1998–2011 (P2), but that this is not statistically significant, unlike the decline in LR rainfall over the same period. The decadal change in MJO123 count explains only ~14% of the decline in LR rainfall. A similar level of variance can be attributed to mean MJO amplitude.

We have demonstrated evidence of a control of MJO123 frequency from an SST gradient spanning the central and eastern Pacific. A dipole between two dominant SST regions of significant correlation with the MAM MJO123 counts was shown to exist, which we have quantified through a new SST index (A1 − A2). The strongest relationship between this dipole and the MJO exists across FM ($\rho = 0.53$, $\rho_{dt} = 0.52$), but we have shown that a significant relationship is present between the MAM MJO and SSTs in all boreal winter months preceding the long rains.

To our knowledge, such a relationship with MJO phases 1–3 has not previously been reported. Roxy et al. (2019) have shown that increased Indo-Pacific warm-pool area increases the duration of MJO events in phases 4–6 during boreal winter, at the expense of phases 1–3. Our results suggest a different SST dipole anomaly impacts phase counts in boreal spring. The SST gradient A1 − A2 we have related here to the MJO lies east of the zonal gradient over 'western-V' warmpool SSTs previously linked to the LR drying trend, and, in stark contrast to that region, exhibits little decadal variability, explaining only ~15% of the decrease in LR rainfall from P1 to P2.

The FM correlation of the SST gradient A1 − A2 to LR values ($\rho = 0.45$, $\rho_{dt} = 0.49$) is lower than that with the MJO123 count, suggesting that the influence of this Pacific SST gradient on LR precipitation is expressed through control of the MJO. This hypothesis is further supported by evidence of mediation of the A1 − A2 influence through the MJO123 count. Again, this is in contrast to western Pacific SSTs (here, the V1 index), for which we find strong correlation with LR rainfall totals, but little correlation with MJO123, and no evidence of mediation. We have not investigated the detailed mechanisms underpinning the relationships shown here, and this should be a priority for future work, especially in light of recent advances for the OND short rains (Vashisht & Zaitchik, 2022).

The influence of the MJO phase also holds during the SR, with ~30% of interannual variability in both seasons explained by the corresponding MJO123 phase count. Near identical seasonal correlations were found from a novel daily estimate of EA precipitation which accounts for MJO phase variability and linear relationships of rainfall with MJO amplitude; this similarity of correlation highlights the importance of phases 1–3. The model-estimate does however capture a higher proportion of the decadal variability of EA rainfall, explaining ~28% of the observed LR decline between P1 and P2.

The MJO amplitude is typically used to measure the MJO when considering teleconnections to interannual

LR variability. Our results suggest that emphasis should also be placed on the frequency of MJO events across the Indian Ocean (i.e., phases 1–3). Furthermore, the relationship of this frequency to Pacific SSTs (A1 − A2), as found in this paper, offers a potential source of improved MJO predictability itself (Stan et al., 2022). Accordingly, the representation of the relationships detailed in this paper should be investigated in both forecast and climate models. For example, although modelling of both the MJO and EA rainfall has improved in CMIP6 models (MJO propagation especially), persistent biases such as underestimated MJO contributions to variability, and underestimated LR accumulations, remain (Ahn et al., 2020; Bartana et al., 2022; Le et al., 2021; Lyon, 2022). There are substantial uncertainties in climate change projections of the long rains (Rowell, 2019): ensuring that models represent the relationships observed here is an important step towards further reducing such uncertainties.

AUTHOR CONTRIBUTIONS

Ben Maybee: Formal analysis; investigation; methodology; writing – original draft; writing – review and editing. **Neil Ward:** Formal analysis; investigation; methodology; writing – review and editing. **Linda Hirons:** Methodology; writing – review and editing. **John H. Marsham:** Conceptualization; funding acquisition; methodology; writing – review and editing.

ACKNOWLEDGEMENTS

We are grateful to Cathryn Birch for comments on the manuscript, and to Richard Keane for comments on the methodology. We also thank two anonymous reviewers for their reviews, which have improved the content of the paper, and in particular for their suggestion of testing mediation hypotheses. The CHIRPS rainfall dataset can be freely accessed at https://data.chc.ucsb.edu/products/CHIRPS-2.0/global_daily/netcdf/p05/. The BoM MJO RMM index is available at http://www.bom.gov.au/climate/mjo/graphics/rmm.74toRealtime.txt, while NOAA ENSO indices may be accessed from https://www.cpc.ncep.noaa.gov/data/indices/sstoi.indices. BM and JHM acknowledge support from the FCDO/NERC HyCRISTAL project (grant NE/M02038X/1). LCH and JHM were supported by the Global Challenges Research Fund, grant NE/P021077/1 (GCRF African SWIFT). LCH was also supported by NERC NCAS International Collaboration NE/X0062631.

ORCID

Ben Maybee https://orcid.org/0000-0001-7834-9489
Neil Ward https://orcid.org/0000-0003-1385-0349

ENDNOTE

[1] Due to the NOAA ENSO index time-period, correlations reported in this paragraph are calculated from 1982, rather than 1981.

REFERENCES

Ahn, M.-S., Kim, D., Kang, D., Lee, J., Sperber, K.R., Gleckler, P.J. et al. (2020) MJO propagation across the maritime continent: are CMIP6 models better than CMIP5 models? *Geophysical Research Letters*, 47, e2020GL087250.

Bahaga, T.K., Fink, A.H. & Knippertz, P. (2019) Revisiting interannual to decadal teleconnections influencing seasonal rainfall in the Greater Horn of Africa during the 20th century. *International Journal of Climatology*, 39, 2765–2785.

Bartana, H., Garfinkel, C., Shamir, O. & Rao, J. (2022) Projected future changes in the equatorial wave spectrum in CMIP6. *Climate Dynamics*. Available from: https://doi.org/10.1007/s00382-022-06510-y

Berhane, F. & Zaitchik, B. (2014) Modulation of daily precipitation over East Africa by the Madden–Julian oscillation. *Journal of Climate*, 27, 6016–6034.

Black, E., Slingo, J. & Sperber, K.R. (2003) An observational study of the relationship between excessively strong short rains in coastal East Africa and Indian Ocean SST. *Monthly Weather Review*, 131, 74–94.

Dasgupta, P., Roxy, M., Chattopadhyay, R., Naidu, C. & Metya, A. (2021) Interannual variability of the frequency of MJO phases and its association with two types of ENSO. *Scientific Reports*, 11, 1–16.

de Andrade, F.M., Young, M.P., MacLeod, D., Hirons, L.C., Woolnough, S.J. & Black, E. (2021) Subseasonal precipitation prediction for Africa: forecast evaluation and sources of predictability. *Weather and Forecasting*, 36, 265–284.

Dunning, C.M., Black, E.C. & Allan, R.P. (2016) The onset and cessation of seasonal rainfall over Africa. *Journal of Geophysical Research: Atmospheres*, 121, 11–405.

FEWS NET Alert. (2021) *The Eastern Horn of Africa faces an exceptional prolonged and persistent agro-pastoral drought sequence*. Available from: https://fews.net/sites/default/files/multi-agency-east-africa-drought-alert-120121.pdf

Finney, D.L., Marsham, J.H., Walker, D.P., Birch, C.E., Woodhams, B.J., Jackson, L.S. et al. (2020) The effect of westerlies on East African rainfall and the associated role of tropical cyclones and the Madden–Julian oscillation. *Quarterly Journal of the Royal Meteorological Society*, 146, 647–664.

Funk, C. (2020) Ethiopia, Somalia and Kenya face devastating drought. *Nature*, 586, 645–646.

Funk, C., Harrison, L., Shukla, S., Pomposi, C., Galu, G., Korecha, D. et al. (2018) Examining the role of unusually warm Indo-Pacific sea-surface temperatures in recent African droughts. *Quarterly Journal of the Royal Meteorological Society*, 144, 360–383.

Funk, C. & Hoell, A. (2015) The leading mode of observed and CMIP5 ENSO-residual sea surface temperatures and associated changes in Indo-Pacific climate. *Journal of Climate*, 28, 4309–4329.

Funk, C., Hoell, A., Shukla, S., Blade, I., Liebmann, B., Roberts, J.B. et al. (2014) Predicting East African spring droughts using Pacific and Indian Ocean sea surface temperature indices. *Hydrology and Earth System Sciences*, 18, 4965–4978.

Funk, C., Pedreros, D., Nicholson, S., Hoell, A., Korecha, D., Galu, G. et al. (2019) Examining the potential contributions of extreme "Western V" sea surface temperatures to the 2017 March–June East African Drought. *Bulletin of the American Meteorological Society*, 100, S55–S60.

Funk, C., Peterson, P., Landsfeld, M., Pedreros, D., Verdin, J., Shukla, S. et al. (2015) The climate hazards infrared precipitation with stations—a new environmental record for monitoring extremes. *Scientific Data*, 2, 1–21.

Hillbruner, C. & Moloney, G. (2012) When early warning is not enough—lessons learned from the 2011 Somalia famine. *Global Food Security*, 1, 20–28.

Hirons, L. & Turner, A. (2018) The impact of Indian Ocean mean-state biases in climate models on the representation of the East African short rains. *Journal of Climate*, 31, 6611–6631.

Hoell, A. & Funk, C. (2014) Indo-Pacific sea surface temperature influences on failed consecutive rainy seasons over eastern Africa. *Climate Dynamics*, 43, 1645–1660.

Hogan, E., Shelly, A. & Xavier, P. (2015) The observed and modelled influence of the Madden–Julian oscillation on East African rainfall. *Meteorological Applications*, 22, 459–469.

Katz, R.W. & Brown, B.G. (1991) The problem of multiplicity in research on teleconnections. *International Journal of Climatology*, 11, 505–513.

Kilavi, M., MacLeod, D., Ambani, M., Robbins, J., Dankers, R., Graham, R. et al. (2018) Extreme rainfall and flooding over central Kenya including Nairobi city during the long-rains season 2018: causes, predictability, and potential for early warning and actions. *Atmosphere*, 9, 472.

Kimani, M., Hoedjes, J.C. & Su, Z. (2020) An assessment of MJO circulation influence on Air–Sea interactions for improved seasonal rainfall predictions over East Africa. *Journal of Climate*, 33, 8367–8379.

Kolstad, E.W. & MacLeod, D. (2022) Lagged oceanic effects on the East African short rains. *Climate Dynamics*, 59, 1043–1056.

Le, P.V., Guilloteau, C., Mamalakis, A. & Foufoula-Georgiou, E. (2021) Underestimated MJO variability in CMIP6 models. *Geophysical Research Letters*, 48, e2020GL092244.

Liebmann, B., Bladé, I., Funk, C., Allured, D., Quan, X.-W., Hoerling, M. et al. (2017) Climatology and interannual variability of boreal spring wet season precipitation in the eastern Horn of Africa and implications for its recent decline. *Journal of Climate*, 30, 3867–3886.

Liebmann, B., Hoerling, M.P., Funk, C., Bladé, I., Dole, R.M., Allured, D. et al. (2014) Understanding recent eastern Horn of Africa rainfall variability and change. *Journal of Climate*, 27, 8630–8645.

Liebmann, B. & Smith, C.A. (1996) Description of a complete (interpolated) outgoing longwave radiation dataset. *Bulletin of the American Meteorological Society*, 77, 1275–1277.

Liu, F., Zhou, L., Ling, J., Fu, X. & Huang, G. (2016) Relationship between SST anomalies and the intensity of intraseasonal variability. *Theoretical and Applied Climatology*, 124, 847–854.

Lyon, B. (2014) Seasonal drought in the Greater Horn of Africa and its recent increase during the March–May long rains. *Journal of Climate*, 27, 7953–7975.

Lyon, B. (2022) Biases in sea surface temperature and the annual cycle of Greater Horn of Africa rainfall in CMIP6. *International Journal of Climatology*, 42, 4179–4186.

Lyon, B. & DeWitt, D.G. (2012) A recent and abrupt decline in the East African long rains. *Geophysical Research Letters*, 39, L02702.

MacLeod, D. (2019) *Seasonal forecast skill over the Greater Horn of Africa: a verification atlas of System 4 and SEAS5. Part 1: Precipitation*. Available from: https://www.ecmwf.int/node/18906

MacLeod, D.A., Dankers, R., Graham, R., Guigma, K., Jenkins, L., Todd, M.C. et al. (2021) Drivers and subseasonal predictability of heavy rainfall in equatorial East Africa and relationship with flood risk. *Journal of Hydrometeorology*, 22, 887–903.

MacLeod, D.A., Graham, R., O'Reilly, C., Otieno, G. & Todd, M. (2021) Causal pathways linking different flavours of ENSO with the Greater Horn of Africa short rains. *Atmospheric Science Letters*, 22, e1015.

Madden, R.A. & Julian, P.R. (1971) Detection of a 40–50 day oscillation in the zonal wind in the tropical Pacific. *Journal of Atmospheric Sciences*, 28, 702–708.

Madden, R.A. & Julian, P.R. (1972) Description of global-scale circulation cells in the tropics with a 40–50 day period. *Journal of Atmospheric Sciences*, 29, 1109–1123.

Nicholson, S.E. (2014) The predictability of rainfall over the Greater Horn of Africa. Part I: Prediction of seasonal rainfall. *Journal of Hydrometeorology*, 15, 1011–1027.

Nicholson, S.E. (2017) Climate and climatic variability of rainfall over eastern Africa. *Reviews of Geophysics*, 55, 590–635.

Omeny, P.A., Ogallo, L., Okoola, R., Hendon, H. & Wheeler, M. (2008) East African rainfall variability associated with the Madden–Julian oscillation. *Journal of Kenya Meteorological Society*, 2, 105–114.

Pang, B., Chen, Z., Wen, Z. & Lu, R. (2016) Impacts of two types of El Niño on the MJO during boreal winter. *Advances in Atmospheric Sciences*, 33, 979–986.

Pohl, B. & Camberlin, P. (2006a) Influence of the Madden–Julian oscillation on East African rainfall. I: Intraseasonal variability and regional dependency. *Quarterly Journal of the Royal Meteorological Society*, 132, 2521–2539.

Pohl, B. & Camberlin, P. (2006b) Influence of the Madden–Julian oscillation on East African rainfall: II. March–May season extremes and interannual variability. *Quarterly Journal of the Royal Meteorological Society*, 132, 2541–2558.

Pohl, B. & Matthews, A.J. (2007) Observed changes in the lifetime and amplitude of the Madden–Julian oscillation associated with interannual ENSO sea surface temperature anomalies. *Journal of Climate*, 20, 2659–2674.

Rayner, N.A.A., Parker, D.E., Horton, E.B., Folland, C.K., Alexander, L.V., Rowell, D.P. et al. (2003) Global analyses of sea surface temperature, sea ice, and night marine air temperature since the late nineteenth century. *Journal of Geophysical Research: Atmospheres*, 108, 4407.

Rowell, D.P. (2019) An observational constraint on CMIP5 projections of the East African long rains and southern Indian Ocean warming. *Geophysical Research Letters*, 46, 6050–6058.

Rowell, D.P., Booth, B.B.B., Nicholson, S.E. & Good, P. (2015) Reconciling past and future rainfall trends over East Africa. *Journal of Climate*, 28, 9768–9788.

Roxy, M., Dasgupta, P., McPhaden, M.J., Suematsu, T., Zhang, C. & Kim, D. (2019) Twofold expansion of the Indo-Pacific warm pool warps the MJO life cycle. *Nature*, 575, 647–651.

Sheffield, J., Wood, E.F., Chaney, N., Guan, K., Sadri, S., Yuan, X. et al. (2014) A drought monitoring and forecasting system for sub-Sahara African water resources and food security. *Bulletin of the American Meteorological Society*, 95, 861–882.

Slingo, J., Rowell, D., Sperber, K. & Nortley, F. (1999) On the predictability of the interannual behaviour of the Madden–Julian oscillation and its relationship with El Niño. *Quarterly Journal of the Royal Meteorological Society*, 125, 583–609.

Stan, C., Zheng, C., Chang, E.K.-M., Domeisen, D.I., Garfinkel, C.I., Jenney, A.M. et al. (2022) Advances in the prediction of MJO Teleconnections in the S2S forecast systems. *Bulletin of the American Meteorological Society*, 103, E1426–E1447.

Suematsu, T. & Miura, H. (2018) Zonal SST difference as a potential environmental factor supporting the longevity of the Madden–Julian oscillation. *Journal of Climate*, 31, 7549–7564.

Vashisht, A. & Zaitchik, B. (2022) Modulation of East African boreal fall rainfall: combined effects of the Madden–Julian oscillation (MJO) and El Niño–Southern oscillation (ENSO). *Journal of Climate*, 35, 2019–2034.

Vellinga, M. & Milton, S.F. (2018) Drivers of interannual variability of the East African "long rains". *Quarterly Journal of the Royal Meteorological Society*, 144, 861–876.

Wainwright, C.M., Finney, D.L., Kilavi, M., Black, E. & Marsham, J.H. (2021) Extreme rainfall in East Africa, October 2019–January 2020 and context under future climate change. *Weather*, 76, 26–31.

Wainwright, C.M., Marsham, J.H., Keane, R.J., Rowell, D.P., Finney, D.L., Black, E. et al. (2019) 'Eastern African Paradox' rainfall decline due to shorter not less intense long rains. *NPJ Climate and Atmospheric Science*, 2, 1–9.

Walker, D.P., Birch, C.E., Marsham, J.H., Scaife, A.A., Graham, R. J. & Segele, Z.T. (2019) Skill of dynamical and GHACOF consensus seasonal forecasts of East African rainfall. *Climate Dynamics*, 53, 4911–4935.

Walker, D.P., Marsham, J.H., Birch, C.E., Scaife, A.A. & Finney, D. L. (2020) Common mechanism for interannual and decadal variability in the East African long rains. *Geophysical Research Letters*, 47, e2020GL089182.

Wheeler, M.C. & Hendon, H.H. (2004) An all-season real-time multivariate MJO index: development of an index for monitoring and prediction. *Monthly Weather Review*, 132, 1917–1932.

Wilks, D.S. (2016) "The stippling shows statistically significant grid points": how research results are routinely overstated and overinterpreted, and what to do about it. *Bulletin of the American Meteorological Society*, 97, 2263–2273.

Williams, A.P. & Funk, C. (2011) A westward extension of the warm pool leads to a westward extension of the Walker circulation, drying eastern Africa. *Climate Dynamics*, 37, 2417–2435.

Yang, W., Seager, R., Cane, M.A. & Lyon, B. (2014) The East African long rains in observations and models. *Journal of Climate*, 27, 7185–7202.

Yang, W., Seager, R., Cane, M.A. & Lyon, B. (2015) The annual cycle of East African precipitation. *Journal of Climate*, 28, 2385–2404.

Zaitchik, B.F. (2017) Madden–Julian oscillation impacts on tropical African precipitation. *Atmospheric Research*, 184, 88–102.

SUPPORTING INFORMATION

Additional supporting information can be found online in the Supporting Information section at the end of this article.

How to cite this article: Maybee, B., Ward, N., Hirons, L. C., & Marsham, J. H. (2023). Importance of Madden–Julian oscillation phase to the interannual variability of East African rainfall. *Atmospheric Science Letters*, *24*(5), e1148. https://doi.org/10.1002/asl.1148